Journal of Nanostructure in Chemistry (2023) 13:377–387
https://doi.org/10.1007/s40097-022-00501-5

ORIGINAL RESEARCH

Ultra-bright green carbon dots with excitation-independent fluorescence for bioimaging

Amandeep Singh[1,2] · Zhi Qu[2] · Astha Sharma[3] · Mandeep Singh[4] · Brian Tse[5] · Kostya Ostrikov[1,2] · Amirali Popat[6] · Prashant Sonar[1,2] · Tushar Kumeria[3,6,7]

Received: 10 February 2022 / Accepted: 13 May 2022 / Published online: 23 June 2022

Abstract

Current and future diagnostics urgently need imaging agents that are non-toxic and superior to clinically used small molecule dyes. Herein, we have developed luminescent green light-emitting carbon dots (GCDs) via a single-step hydrothermal reaction using a low-cost chemical precursor, p-toluenesulfonic acid. The GCDs exhibit excitation-independent fluorescence (FL) emission with the photoluminescence quantum yield of 70% and no FL quenching up to 1.25 mg/mL. The GCDs exhibit negligible cytotoxicity up to 250 µg/mL concentration in RAW 264.7 cells. Interestingly, GCDs exhibit an excitation-independent and concentration-dependent fluorescence emission behaviour. In vitro, the peak emission was obtained at 520 nm using the excitation at 430 nm. Whereas FL intensity increased with increasing concentration up to 1.25 mg/mL and a sharp decrease in FL intensity is observed upon further increasing the concentration of GCDs. Upon subcutaneously injecting the GCDs into a euthanized mouse, a similar concentration-dependent FL behaviour is evident. Background autofluorescence hinders the use of the GCDs at 420 nm excitation, however, a strong FL emission at 520 nm can be obtained by exciting subcutaneously injected GCDs at 465 nm—demonstrating excitation-independent emission characteristics. The above results indicate the potential of the non-toxic, low-cost carbon dots for diverse bioimaging applications.

Graphical abstract

Ultra-bright green-emitting carbon dots (GCDs) with photoluminescence quantum yield of 70% were synthesized using p-toluenesulfonic acid and ethylenediamine as precursors. The GCDs were subcutaneously injected into fresh mouse cadaver for fluorescence (FL)bioimaging, showing dose-dependent FL intensity behaviour.

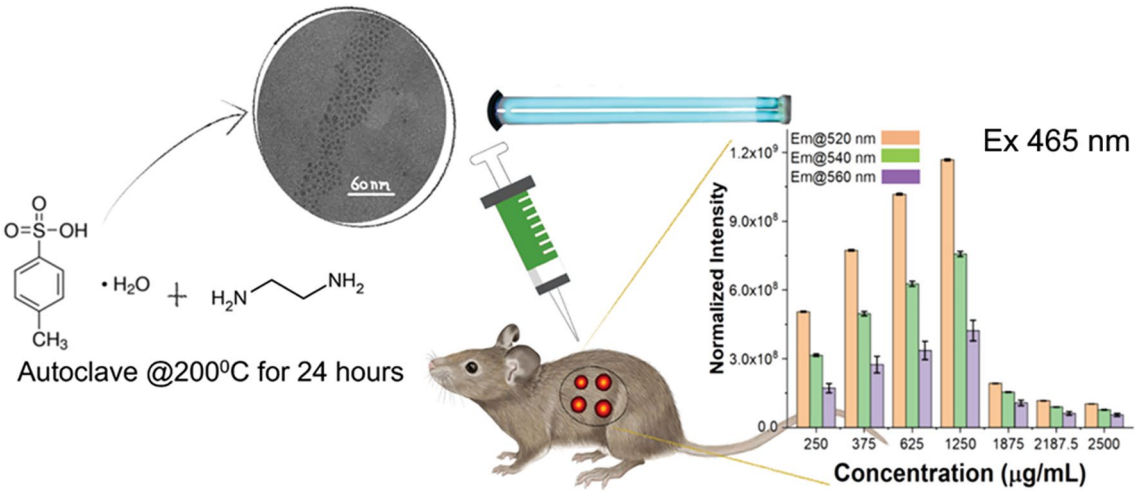

Amandeep Singh and Zhi Qu have contributed equally.

Extended author information available on the last page of the article

Keywords Fluorescence imaging · Quantum dots · Green fluorescent carbon dots · Bioimaging · Theranostics

Introduction

Fluorescence (FL) imaging is one of the most common modalities of clinical imaging [1, 2]. Numerous small molecule dyes (e.g. indocyanine green, fluorescein, methylene blue, and several others) are already approved for clinical use by the United States Food and Drug Administration (US-FDA) and other regulatory bodies [3, 4]. However, small molecule dyes suffer from a short half-life, quenching, and blinking effects in a microsecond (µs) time scale [5, 6]. Therefore, several new fluorescent imaging agents have been developed in the last decade including improved organic small molecules [7–10], conjugated polymers [11, 12], quantum dots [13–16], and other hybrid or nanocomposite materials [17–21]. Among these candidates, nanomaterial-based imaging agents in particular quantum dots have been very successful fluorescent probes [22, 23]. These probes are currently used at various stages of clinical trials (e.g. Cornell dots, Feridex I.V., SonoVue, etc.) for specific imaging of a range of diseases [3, 24]. The key advantages of such imaging agents include high biocompatibility, long circulation half-life, ability to target specific disease sites, and significantly improved signal enhancement [25, 26].

More recently, carbon dots (CDs) have become a popular choice as an imaging agent due to their remarkable biocompatibility and proven biodegradation compared to other inorganic semiconductor quantum dots [27–30]. The fluorescent organic CDs are among the emerging low-cost and promising imaging agents due to their tuneable surface functionality, unique optical properties (e.g. excitation dependent emission), and the ability to use a range of low-cost materials or bio-waste materials as starting precursors for their synthesis [30–32].

Based on the synthesis protocols, starting precursor and attachment of linkers or ligands, the size of the CDs and their emitting properties can be effectively tuned [33, 34]. Researchers have created CDs with a wide range of emission wavelength (i.e. colours) [36–39] that have been utilized in a variety of devices including flexible organic light-emitting diodes [33], environmental sensors [34], bio-targeting and drug delivery [40–43], cellular and subcellular imaging [44, 45] and diagnostic-imaging [46, 47]. These devices have been applied for environmental, physical, and medical use, while several new applications are now emerging based on their unique optoelectronic properties. To be considered as an efficient FL agent for bioimaging that is superior to common dyes, the CDs must have a high photoluminescent quantum yield (PLQY), be made from an abundant and low-cost starting precursor, and have a high Stokes shift between the excitation and the emission wavelengths. Lili Tong et al. developed green-emitting CDs (i.e. GCDs) with a very high PLQY of 90% for long-term lysosome imaging [48]. However, the precursor used in the synthesis of CDs was very expensive Rose Bengal (US$69 per gram) and the material exhibits a small Stokes shift between excitation and emission (20 nm with excitation at 508 nm and peak emission at 528 nm) wavelengths. Songnan et al. synthesized water-soluble CDs using a one-step microwave reactor-based process with an equal amount of citric acid (3 g) and urea (3 g) as starting precursors. The synthesized CDs showed a good stroke shift of 100 nm (excitation/emission 420/520 nm), with an enhanced fluorescent quantum yield of 40%. Thus, the low cost, biocompatibilty, and distinct PL properties proves these C-dots could potentially be produced on an industrial scale as a new fluorescent ink for versatile applications [49]. Xu et al. used tartaric acid and bran as starting precursors to synthesize green light-emitting CDs [50]. The one-pot solvothermal process produces CDs with 46% PLQY. Pei Yang et al. synthesized nitrogen/sulphur co-doped green–yellow emitting CDs using xylose as starting precursor [51]. They used a microwave reactor to synthesize CDs with PLQY of 42%. With poor PLQY and short or fixed Stokes shift in excitation and emission remains a major challenge. Kateshiya et al. synthesized multi-colored (Blue, Green, and Yellow emitting)-CDs using natural precursor, ripe fruit of *Annona squamosal* through an acid oxidation process. The prepared hybrid fluorescent nanosensor were surface functionalized with molybdenum trioxide nanoparticles (MoO_3 NP) to impart selectivity towards ClO^- and were demonstrated for their use as Fl quenching-based sensors to detect ClO^- in water [25].

In this work, we have overcome these challenges and synthesized low-cost GCDs with ultra-high PLQY (70%) from inexpensive starting precursors. Due to the unique single-step sulphur and nitrogen doping during synthesis, the GCDs show an excitation-independent emission characteristic. Our work, to date, is the first report to demonstrate excitation-independent green emission from carbon dots prepared using an inexpensive precursor that costs less than AU$0.04 for 1 g. This ultra-high PLQY enables our GCDs to allow for bioimaging in the same spectral range as background autofluorescence, which is not possible with low PLQY conventional fluorophores and other CDs. The prepared GDs have the potential to enable low-cost FL imaging without the need for more expensive IR imaging systems. In addition, the GCDs were highly cytocompatible at concentrations up to 250 µg/mL with RAW264.7 macrophage cells.

The GCDs displayed a concentration-dependent FL with the highest emission intensity at 1.2 mg/mL concentration. A similar concentration-dependent FL intensity behaviour was observed upon subcutaneous injection of the GCDs into a fresh mouse cadaver. Interestingly, the optimum excitation wavelength for subcutaneously injected GCDs was 465 nm compared to 420 nm for in vitro assessment due to high background autofluorescence at the latter excitation wavelength.

Materials and methods

Materials

p-Toluenesulfonic acid (PTSA) and ethylenediamine were purchased from merk. Aluminum oxide powder (average particle size of fewer than 1 µm) and ethylenediamine were purchased from Sigma Aldrich. All the reagents were of analytical grade and used as supplied.

Synthesis of CDs

To start, 1.7 g of PTSA was dissolved in 40 mL water. This final solution was loaded in an autoclave with 50 mL of inner Teflon container and 2 mL of ethylenediamine was added to this solution [33, 34]. Please note, the reactor was filled with approximately 80% of its capacity to create high autogenous pressure. The Teflon reactor was sealed in the stainless steel autoclave and heated to 200 °C in an oven for 24 h. Next, the autoclave was naturally cooled to room temperature. The obtained product was filtered using a column packed with aluminum oxide absorbent to remove the undesired by-products. The above purification step was repeated several times to obtain the final solution.

Cytocompatibility of CDs

The cytocompatibility of the CDs was assessed with RAW264.7 cells using our well-established protocol [16]. The cells were cultured in DMEM with 10% fetal calf serum, 1% penicillin/streptomycin, and 1% L-glutamine in an incubator at 37 °C with 5% CO_2. Cells were seeded in a 96-well plate with a density of 5000 cells per well overnight before the experiment. Then, the culture medium was replaced with a medium with carbon dots (250, 100, 20, 5, and 1 µg/mL) and cultured for 24 h. At designated time points, cell viability was tested using CellTiter 96® AQ_{ueous} One Solution Cell Proliferation Assay (MTS) kit (Promega) as directed by the manufacturer.

In vitro and ex vivo bioimaging with CDs

The bioimaging capabilities of the CDs were measured using an IVIS® Spectrum optical imaging system (Perkin Elmer, USA) under both in vitro and ex vivo conditions. For in vitro assessment, 20 µL aliquots of CDs at seven different concentrations (250, 375, 625, 1250, 1875, 2187.5, and 2500 µg/mL) in phosphate buffer saline (PBS) were placed on a hydrophobic non-fluorescent black mat then imaged at different combinations of excitation and emission wavelengths. Excitation-dependent fluorescence values were obtained from regions of interest (ROIs) drawn around each aliquot using Living Image software (Perkin Elmer, USA). For ex vivo assessment, 20 µL aliquots of CDs at different concentrations were injected subcutaneously using a 29G needle in freshly euthanized CD-1 mouse cadavers. Approval to use tissues from euthanized mouse was obtained from the University of Queensland (ethics number: ANRFA/TRI/485/18). The mice injected subcutaneously with CDs were imaged at different excitation and emission wavelength combinations like the in vitro assessment to determine the most suitable bioimaging spectral range with the lowest background autofluorescence. Fluorescence intensity was calculated using ROI analysis in Living Image software.

Characterization

Transmission electron microscopy (TEM)

Transmission electron microscopy (TEM) and high-resolution TEM (HRTEM) images of GCDs were collected using a JEOL 2100 TEM (acceleration voltage: 200 kV). For EDX mapping and spectra, a JEOL 2200FS TEM in STEM bright-field mode with a Bruker detector was used.

Absorption spectra

Absorption spectra of GCD were recorded on a Cary 60 G6860A spectrophotometer (Agilent) using water as a suspending medium at concentrations that resulted in absorption below 1 unit.

The Fourier transform infrared (FTIR)

The Fourier transform infrared (FTIR) data were obtained using Bruker ATR using dry powdered GCDs sample.

X-ray photoelectron spectroscopy (XPS)

X-ray photoelectron spectroscopy (XPS) data were acquired using an Axis Supra (Kratos) with aluminum AlKα (hV = 1486.7 eV). For this, a known amount of GCDs were dropped cast on aluminum foil. The GCD samples were grounded with carbon tape to prevent charging during the

measurements. Please note, charge compensation was also used while recording the data.

Photoluminescence emission

Photoluminescence emission of CDs dispersed in water was measured using an Eclipse G9800A (Cary) Fluorescence Spectrophotometer.

Photoluminescence quantum yield measurements

Photoluminescence quantum yield measurements were carried out using the relative PLQY method. Herein, a rhodamine dye with quantum yield of 31% was chosen as the standard reference with known PLQY. Absorbance and FL of standard and GCDs were recorded and PLQY was calculated using Eq. (1) [52].

$$\phi = \phi_{\mathrm{Ref}} X \frac{\frac{\int A_1}{1-10^{-\mathrm{Abs}}} S}{\frac{\int A_2}{1-10^{-\mathrm{Abs}}} R}, \tag{1}$$

where ϕ_{ref} = Quantum yield of reference dye, (0.31 in this case); ϕ = Quantum yield of sample, subscript S is for sample and R is for reference sample. Note, the absorbance of both the reference and sample were kept below 0.05 at the measurement excitation wavelength to minimize re-absorption effects in a 10 mm fluorescence cuvette.

Results and discussion

Structural properties of GCDs

Here, we demonstrate the generation of GCDs using an ultra-low-cost chemical precursor, p-toluenesulfonic acid (PTSA). The GCDs were generated by hydrothermal processing of PTSA in presence of ethylenediamine at 200 °C. The key advantages of using PTSA with ethylenediamine for GCDs fabrication include low cost, single-step doping with S=O and nitrogen groups, and ultra-bright green emission with excitation-independent emission characteristics (Fig. 1).

The prepared GCDs were thoroughly characterized using an array of characterization methods. The TEM images in Fig. 1b show the shape and uniform size distribution of the synthesized GCDs. The inset in Fig. 1b shows a higher magnification image of the same GCDs. The high-resolution TEM presented in Fig. 1c exhibits regular lattice fringes with a fringe width of 0.21 nm, which is very small compared to the graphitic interlayer distance of 0.34 nm. This lattice plane distance points to the presence of (100) diffraction plane of sp^2 graphitic carbon, indicating a tight packing of GCDs lattices [31]. In addition to TEM, the size and dispersity of GCDs were also measured using the dynamic light scattering (Fig. S1, Electronic Supplementary Information), which reported a size distribution between 3.6 and 7.3 nm with a polydispersity index of 0.254, which informs of the narrow particle size distribution of the CDs. A narrow size distribution is important for quantum confinement based emitters such as CDs because of a strong dependence of emission wavelength on particle size. A broad particle size distribution is associated with a wider emission spectral band and reduced imaging potential of the CDs [35]. Furthermore, the surface zeta-potential of GCDs determined by the DLS was close to − 18 mV which plays a major role in their colloidal stability. The colloidal stability of GCDs was also explored by measuring the hydrodynamic size of GCDs stored in deionized water (pH 6.8) at room temperature (22–25 °C) over a period of 4 months using DLS. The particle size increased very slightly (Fig. S1), indicating the long-term aqueous storage stability of the prepared GCDs.

Optical and chemical properties of GCDs

The optical properties of GCDs were investigated to understand the associated emission centers. The UV–Visible absorption spectrum of GCDs in Fig. 1d shows strong absorbance at 410 nm. This strong 410 nm absorption peak can be attributed to the S=O molecular entity imparted by the PTSA precursor, since it has sulphonic acid group present in its chemical structure. Similar observations have been made with CDs synthesized using precursors with S=O groups or in presence of sulphuric acid [53, 54]. Furthermore, the FL emission at various excitation wavelengths ranging from 360 to 500 nm is shown in Fig. 1d, e. The CDs display an excitation-independent FL emission with the peak FL intensity when excited at 420 nm. The small dependency of emission even at the higher excitation wavelength (Fig. 1e) of GCDs can be associated with the uniform size distribution and a similar kind of functional group present on the surface with defects being passivated. The photoluminescence quantum yield (PLQY) of these GCDs was close to 70% that has never been demonstrated for carbon dots that display an excitation-independent green emission. More broadly, the high PLQY of the prepared GCDs can be attributed to narrow size distribution which results in small the re-absorption of emission by bigger size particles and the starting precursor with aromatic ring helps in formation of CDs with properly defined structure with minimum side products and impurities. The Absorbance and FL emission spectrum of rhodamine dye used for measuring the relative PLQY of GCDs are provide in Fig. S2. The various studies are summarized in Table S1 (Electronic Supplementary Information). The important role of ligands on the surface of CDs in determining their FL behavior is well

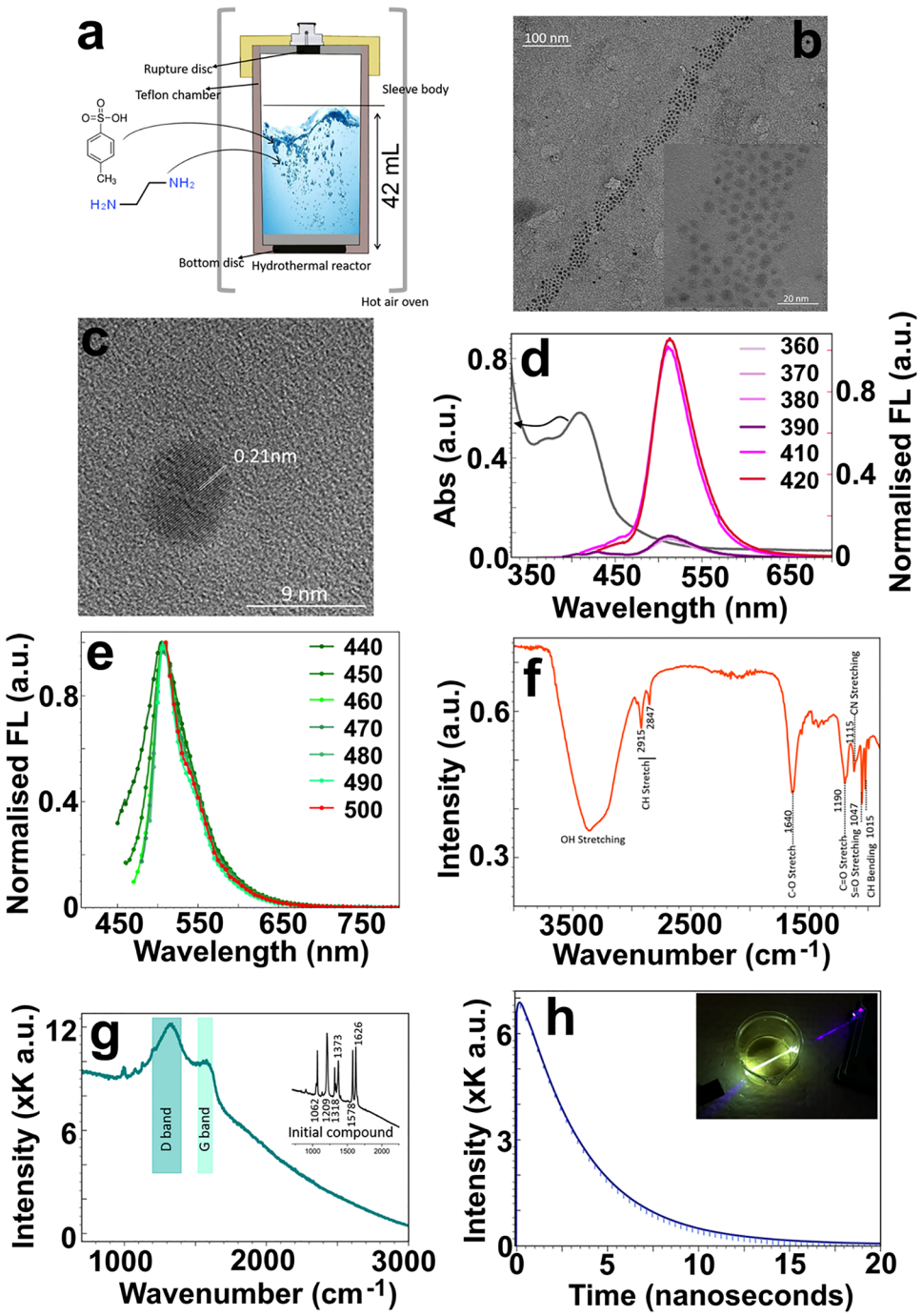

Fig. 1 **a** A schematic of hydrothermal synthesis of GCDs. The initial precursors are mixed in a Teflon container which is filled with 70–80% water to create enough autogenous pressure for the breakdown of precursor and formation of CDS (in a 50 mL reactor). The Teflon reactor is sealed inside stainless steel container to form a pressurized system and kept inside a hot air oven for heating. **b** TEM of GCDs (scale bar: 100 nm). Inset shows a higher magnification TEM of the same GCDs (scale bar: 20 nm). **c** HRTEM of GCDs with measurement of the graphitic lattice. **d** A UV–Visible spectrum of GCDs showing a strong absorption peak around 420 nm. The FL emission spectrum of GCD between an excitation wavelength range of 360–420 nm with minimal effect of the excitation wavelength on the emission wavelength peak. **e** The FL spectrum of GCDs excited at a higher wavelength from 440 to 500 nm further demonstrating excitation wavelength-independent emission. **f** FTIR spectrum of GCDs showing characteristic vibration bands for key functional groups imparted because of the precursors used during the synthesis. **g** Raman spectrum of GCDs deposited on a steel substrate (excitation: 785 nm). The insert shows the Raman spectra of chemical precursor (PTSA) at the same 785 nm excitation. **h** Time-resolved FL decay measured for GCDs. The inset shows a digital photograph of GCDs solution excited by a 420 nm Laser, where strong green FL can be visually detected

established [33]. For the prepared GCDs, the presence of S=O molecular entity, introduced by the starting precursor, was confirmed by FTIR analysis that showed strong vibration at 1047 cm^{-1} and small stretching vibration peaks between 1300 and 1410 cm^{-1} that typically correspond to S=O stretching mode (Fig. 1f). The C–H bending vibration and the corresponding C–H stretching dual-bands appear at1015 cm^{-1}, and at 2847 and 2915 cm^{-1}, respectively. A hydroxyl group (O–H) stretching at 330 cm^{-1} is present due to the surface hydroxyl groups because of the water-based synthesis process. In addition, the nitrogen doping was confirmed by a C–N stretching vibration band at 1115 cm^{-1}.

To study the surface functionalities, the Raman signal of GCDs was recorded (Fig. 1g). The *D* band located at 1317 cm^{-1} is a signature of sp^3 orbital vibration, whereas the G band at 1582 cm^{-1} is attributed to sp^2 orbital vibration [54]. The ratio of the intensity of *D* band to *G* band (I_D/I_G) provides useful information about sp^3/sp^2 characteristics of CDs. The I_D/I_G ratio of 1.2 indicates a high proportion of surface defects in GCDs due to sulfur-containing moiety.

The insert in Fig. 1g shows the Raman signal of PTSA precursor. The disappearance of the characteristic Raman peaks of PTSA and appearance of characteristic graphitic D and G band clearly indicating the formation of GCDs has been completed. To investigate the emission centers of GCDs, the PL decay curve under 470 nm pulsed laser (Fig. 1h) was obtained. The PL decay curves of GCDs can be well fitted with a single-component exponential decay model (Fig. 1h), suggesting the presence of a single emission center. The average lifetime of GCDs comes out to be 3.09 ns. Since there is no prolonged emission, indicating the absence of deeper trap states due to defects. The fast σ^*–n and π^*–n transitions are associated with emissions from functional groups indicating the role of the S=O group in green fluorescence [34].

XPS analysis was conducted to further analyze the elemental bonding states in the surface layer of GCDs, (Fig. 2). The XPS survey spectrum shown in Fig. 2a indicates various chemical components of the GCD, which was comprised mainly of carbon (53.57%) and oxygen (38.53%) with less than 5% amounts of other elements such as nitrogen, which was at 2.45%, sulfur at 3.81%, and sodium at 1.64%. The presence of nitrogen (2.45%), as shown in the XPS, can be attributed to the use of ethylenediamine as a doping agent. The atomic resolution chemical mapping in STEM, confirms that nanoparticles present are carbon with oxygen, nitrogen, and sulfur on its surface (Fig. S3). The chemical structure of PTSA precursor (Fig. 1a) shows that it can serve as for carbon, oxygen, and sulfur content observed in the XPS. Whereas the small amount (1.64%) of sodium (Na1s) is likely an impurity arising from the chemicals or reagents used in the synthesis of GCDs.

Deconvolution of the high-resolution C1s spectrum of GCD in Fig. 2b affords three peaks. The strongest peak

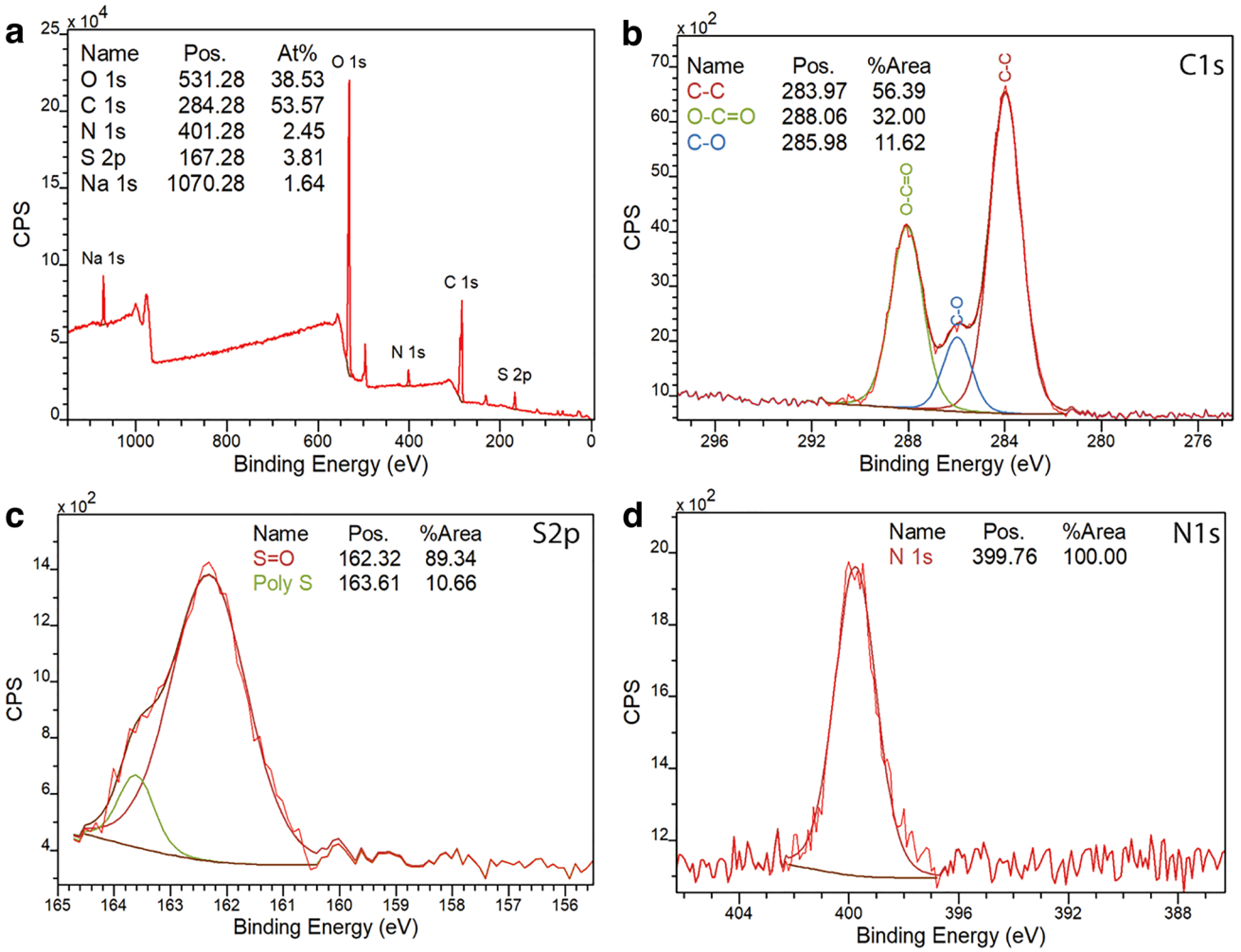

Fig. 2 Surface properties GCDs investigated using XPS **a** a survey spectrum with inset table providing the compositional data. **b** High-resolution C1s XPS spectra of GCDs with three major peaks. **c** High-resolution S2p XPS spectra of GCDs fitted with two prominent peaks. And **d** high-resolution N1s XPS spectra of GCDs

(283.97 eV) can be attributed to C–C bond, while the peak at 288.06 eV corresponds to O–C=O bond. The weakest peak (285.98 eV) can be ascribed to C–O bond. The deconvoluted high-resolution S2p spectrum of GCDs (Fig. 2c) fits two peaks with a stronger peak at 162.32 eV, which can be attributed to the S=O bond and a peak at 163.61 eV from a poly sulfur atom. The presence of this S=O moiety is believed as the reason for the green emission of GCDs. The presence of S=O moiety was also confirmed by FTIR shown in Fig. 1f. Whereas, only a single peak at 399.76 eV can be fitted to the high-resolution N1s spectrum of GCDs (Fig. 2d), which can be attributed to NH_2 moiety.

In vitro cytocompatibility of GCDs

The in vitro cell viability of carbon dots was examined using a macrophage cell line RAW 264.7 (RAW cells), which are widely used for determining the cytocompatibility of nanomaterials [17, 56, 57]. The RAW cells grew normally after exposure to carbon dots even up to concentrations as high as 250 µg/mL. Figure S4 shows above 100% cell viability after 24 h exposure to GCDs compared with PBS control measured using MTS assay. As expected, the results showed that the GCDs did not inhibit cell growth, compared with control, indicating good cytocompatibility.

In vitro bioimaging using GCDs

In vitro imaging using GCDs provided essential details of appropriate excitation and emission wavelengths, and concentration-dependent FL behaviour of GCDs. Seven different concentrations of GCDs starting from 250 µg/mL to 2.5 mg/mL were prepared and imaged using IVIS® live animal imaging system at nine different combinations of excitation and emission wavelengths (Fig. 3a–i). After adjusting the image intensity so that the negative control (PBS) showed the zero FL intensity, the FL from the samples was quantified over the spectral region of interest. The analysis showed the maximum in vitro FL at an excitation wavelength of 430 nm and an emission wavelength of 520 nm as shown in the heat map in Fig. 3j.

Interestingly, an increase in FL was observed for GCDs concentrations of up to 1.25 mg/mL and a drastic decrease in FL for all the tested concentrations above 1.25 mg/mL (*i.e.* 1.86, 2.19, and 2.5 mg/mL) as presented in Fig. S5. This trend was observed for all the sets of excitation and emission wavelength combinations assessed in this study. These results could potentially be explained by the increased collision of GCDs at concentrations beyond 1.25 mg/mL that leads to FL quenching. This phenomenon has been observed previously with CDs, where a steep decline in FL occurs beyond a concentration and this is attributed to the increased collision of CDs that leads to non-radiative transfer of energy [58, 59]. A detailed mechanistic exploration of concentration-dependent FL bahaviour of CDs produced from citric acid as precursor was carried out in our recent article, where multicolour FL emission from nitrogen-doped CDs was revealed to be dependent on CDs' concentration [58]. These fundamental understandings of the compositional and concentration relationship with FL behaviour from CDs underpin the work presented in this article. It is worth noting that the surface functional groups of GCDs provide reasonable resistance to fluorescence quenching below 1.25 mg/mL, hence additional linkers were not used to further stabilize the GCDs. Typically, CDs show collision quenching at much lower concentrations (at µg/mL levels) [58]. Moreover, further stabilization will increase the cost of production of such GCDs and add additional steps in the synthesis.

Bioimaging with subcutaneously injected GCDs

After in vitro cytotoxicity measurement and bioimaging of GCDs at different concentrations, GCDs were subcutaneously (SC) injected into a cadaver of freshly euthanized mice. Each mouse was injected with four different concentrations of GCDs and respective controls for fluorescence imaging. First, the best combination of FL excitation and emission wavelength was determined for SC injected GCDs. This important experiment, aided in the selection of the most optimal excitation and emission wavelengths, which were starkly different from that of the in vitro imaging experiment. As observed in Figs. S6 and S7, an excitation wavelength of 465 nm and an emission wavelength of 520 nm provided the highest FL of GCDs with the lowest background autofluorescence from mice skin that was observed for 430 nm excitation wavelength. While the 500 nm excitation neither displayed FL from the GCDs nor a strong background autofluorescence from the skin. These results can be attributed to the excitation-independent FL emission characteristics of the GCDs. Autofluorescence of skin tissue at UV-blue excitation wavelengths and the low excitation light penetration depth is well known and supports our data [60, 61]. It is worth pointing out that despite a low penetration depth of 465 nm in the skin, a strong FL signal from GCDs was observed and can be attributed to their high PLQY. Figure S8 shows FL from different concentrations of GCDs upon SC injection. Similar to the in vitro imaging, an increase in FL up to 1.2 mg/mL concentration of GCDs was observed, which was followed by a decrease with increasing concentrations of GCDs (Figure S5, Supporting Information). As expected, the spot injected with PBS control (Spot 1 in Fig. 4a) did not show any FL. After in vitro cytotoxicity measurement and bioimaging of GCDs at different concentrations, GCDs were

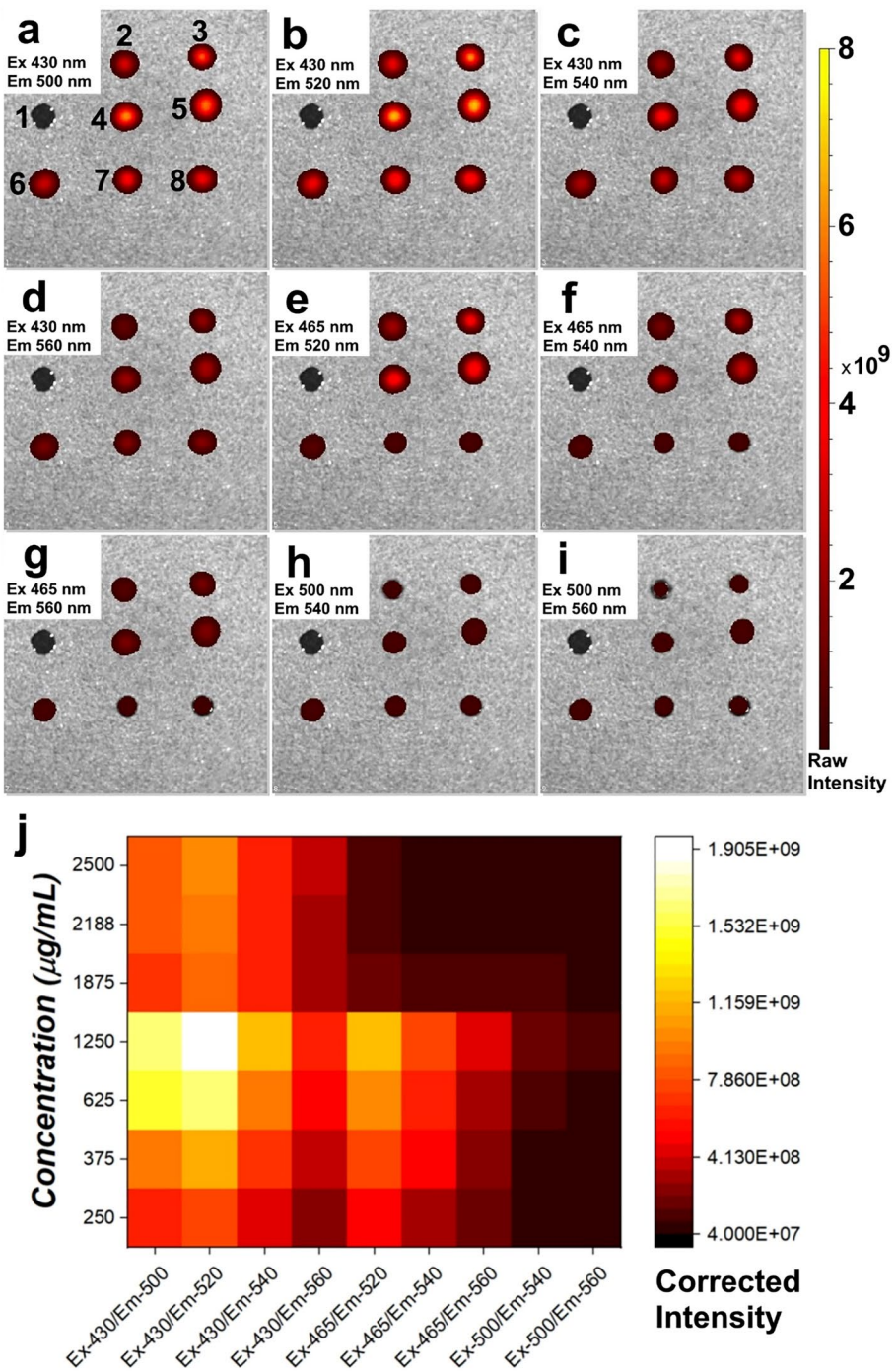

Fig. 3 **a**–**i** In vitro IVIS® (imaging of GCDs at different concentrations and different excitation/emission wavelength combinations. Drops (100 µL) of GCDs in PBS were aspirated on a non-fluorescent black paper. The number next to the drop is representative of the concentrations such that **1**: PBS, **2**: 250 µg/mL, **3**: 375 µg/mL, **4**: 625 µg/mL, **5**: 1250 µg/mL, **6**: 1875 µg/mL, **7**: 2187.5 µg/mL, and **8**: 2500 µg/mL. Note, the order of drops in all the panels from **a**–**i** is the same. **j** A heat map of corrected intensity (i.e. Sample intensity—PBS intensity) was obtained from the in vitro IVIS® FL images in **a**–**i**. The FL is presented as radiance efficiency with unit [p/s/cm^2/sr]/[µW/cm^2]

subcutaneously (SC) injected into a cadaver of freshly euthanized mice. Each mouse was injected with four different concentrations of GCDs and respective controls for fluorescence imaging. First, the best combination of FL excitation and emission wavelength was determined for SC injected GCDs. This important experiment, aided in the selection of the most optimal excitation and emission wavelengths, which were starkly different from that of the in vitro imaging experiment.

Conclusion

In summary, ultra-bright Green Fluorescent Carbon Dots (GCDs) have been synthesized using a high-yielding single-step hydrothermal process. The surface analysis by XPS, reveals the presence of the S=O group on the surface of GCDs, resulting in the excitation-independent green emission. Synthesized GCDs are highly cytocompatible at a dose as high as 250 µg/mL. Furthermore, the steric effects due to the same

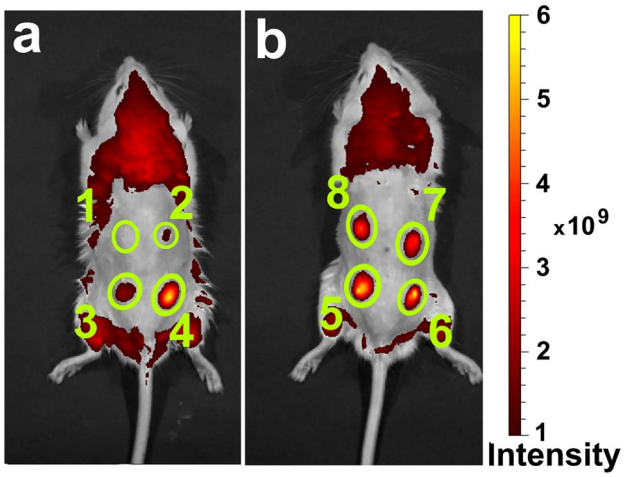

Fig. 4 IVIS® imaging of GCDs at different 465 nm excitation and 520 nm emission wavelength combination for **a** PBS control and three concentrations (250, 375, and 625 µg/mL) of GCDs. **b** four concentrations (250, 375, and 625 µg/mL) of GCDs. Subcutaneous injection spots are marked with number 1to 8 in. Spot 1 is PBS (i.e. 0 µg/mL), Spot 2 is 250 µg/mL of GCDs, Spot 2 is 375 µg/mL of GCDs, Spot 2 is 650 µg/mL of GCDs, Spot 5 is 1250 µg/mL of GCDs, Spot 6 is 1875 µg/mL of GCDs, Spot 7 is 2187.5 µg/mL of GCDs, and Spot 8 is 2500 µg/mL of GCDs. The FL is presented as radiance efficiency with unit [p/s/cm^2/sr]/[µW/cm^2]

surface group impart the GCDs resistance to emission quenching below a concentration of 1.2 mg/mL. In vitro imaging demonstrated that GCDs fluorescence across a range of emission wavelengths from multiple excitation wavelengths with the strongest FL signal achieved from the Ex 430 nm/Em 520 nm wavelength combination. Importantly, FL intensity was dose dependent with the peak signals attained at 1.25 mg/mL and drops beyond this concentration due to collision quenching. When subcutaneously injected in freshly euthanized mice, the GCDs also provided strong FL with the maximum signals at the Ex 465 nm/Em 520 nm wavelength combination. The need for a higher excitation wavelength ex-vivo arises from the strong background autofluorescence, which was reduced drastically at 465 nm for the GCDs. The reliable observation of the GCDs fluorescence through the animal tissue highlights its potential utility in biomedical imaging applications.

Supplementary Information The online version contains supplementary material available at https://doi.org/10.1007/s40097-022-00501-5.

Acknowledgements T. K. acknowledges the support from the National Health and Medical Research Council of Australia for Early Career Fellowship (GNT1143296), Australian Research Council for Discovery Project (DP200102723), and the University of New South Wales for support and Scientia Grant. A. P. acknowledges Career Development Fellowship NHMRC and strategic research funds from School of Pharmacy and Mater Research Institute. P.S. is thankful to QUT for financial support from the Australian Research Council (ARC) for the Future Fellowship (FT130101337) and QUT core funding (QUT/322120-0301/07). The authors acknowledge TRI for providing an excellent research environment and core facilities that enabled this research, particularly Preclinical Imaging. TRI is supported by grants from the Australian and Queensland Governments.

Funding Open Access funding enabled and organized by CAUL and its Member Institutions.

References

1. Hananya, N., Shabat, D.: Recent advances and challenges in luminescent imaging: bright outlook for chemiluminescence of dioxetanes in water. ACS Cent. Sci. **5**, 949–959 (2019)
2. Cai, Y., Si, W., Huang, W., Chen, P., Shao, J., Dong, X.: Organic dye based nanoparticles for cancer phototheranostics. Small **14**, 1704247 (2018)
3. Slooter, M., Janssen, A., Bemelman, W., Tanis, P., Hompes, R.: Currently available and experimental dyes for intraoperative near-infrared fluorescence imaging of the ureters: a systematic review. Tech. Coloproctol. **23**, 305–313 (2019)
4. Coll, J.-L.: Cancer optical imaging using fluorescent nanoparticles. Nanomedicine **6**, 7–10 (2011)
5. Cannone, F., Chirico, G., Bizzarri, A.R., Cannistraro, S.: Quenching and blinking of fluorescence of a single dye molecule bound to gold nanoparticles. J. Phys. Chem. B. **110**, 16491–16498 (2006)
6. Mukkamala, R., Lindeman, S.D., Kragness, K.A., Shahriar, I., Srinivasarao, M., Low, P.S.: Design and characterization of fibroblast activation protein targeted pan-cancer imaging agent for fluorescence-guided surgery of solid tumors. J. Mater. Chem. B **10**(12), 2038–2046 (2022)
7. Hu, Z., Fang, C., Li, B., Zhang, Z., Cao, C., Cai, M., Su, S., Sun, X., Shi, X., Li, C.: First-in-human liver-tumour surgery guided by multispectral fluorescence imaging in the visible and near-infrared-I/II windows. Nat. Biomed. Eng. **4**, 259–271 (2020)
8. Li, J.-B., Liu, H.-W., Fu, T., Wang, R., Zhang, X.-B., Tan, W.: Recent progress in small-molecule near-IR probes for bioimaging. Trends Chem. **1**, 224–234 (2019)
9. Zhou, H., Yi, W., Li, A., Wang, B., Ding, Q., Xue, L., Zeng, X., Feng, Y., Li, Q., Wang, T.: Specific small-molecule NIR-II fluorescence imaging of osteosarcoma and lung metastasis. Adv. Healthc. Mater. **9**, 1901224 (2020)
10. Zeng, X., Xiao, Y., Lin, J., Li, S., Zhou, H., Nong, J., Xu, G., Wang, H., Xu, F., Wu, J.: Near-infrared II dye-protein complex for biomedical imaging and imaging-guided photothermal therapy. Adv. Healthc. Mater. **7**, 1800589 (2018)
11. Li, S., Chen, T., Wang, Y., Liu, L., Lv, F., Li, Z., Huang, Y., Schanze, K.S., Wang, S.: Conjugated polymer with intrinsic alkyne units for synergistically enhanced Raman imaging in living cells. Angew. Chem. Int. Ed. **56**, 13455–13458 (2017)

12. Piwoński, H., Michinobu, T., Habuchi, S.: Controlling photophysical properties of ultrasmall conjugated polymer nanoparticles through polymer chain packing. Nat. Commun. **8**, 1–10 (2017)
13. Chinnathambi, S., Shirahata, N.: Recent advances on fluorescent biomarkers of near-infrared quantum dots for in vitro and in vivo imaging. Sci. Technol. Adv. Mater. **20**, 337–355 (2019)
14. Tang, H., Yang, S.-T., Yang, Y.-F., Ke, D.-M., Liu, J.-H., Chen, X., Wang, H., Liu, Y.: Blood clearance, distribution, transformation, excretion, and toxicity of near-infrared quantum dots Ag_2Se in mice. ACS Appl. Mater. Interfaces **8**, 17859–17869 (2016)
15. Tan, T.T., Selvan, S.T., Zhao, L., Gao, S., Ying, J.Y.: Size control, shape evolution, and silica coating of near-infrared-emitting PbSe quantum dots. Chem. Mater. **19**, 3112–3117 (2007)
16. Wegner, K.D., Hildebrandt, N.: Quantum dots: bright and versatile in vitro and in vivo fluorescence imaging biosensors. Chem. Soc. Rev. **44**, 4792–4834 (2015)
17. Chaudhary, Z., Khan, G.M., Abeer, M.M., Pujara, N., Tse, B.W.-C., McGuckin, M.A., Popat, A., Kumeria, T.: Efficient photoacoustic imaging using indocyanine green (ICG) loaded functionalized mesoporous silica nanoparticles. Biomater. Sci. **7**, 5002–5015 (2019)
18. Kuang, Y., Zhang, K., Cao, Y., Chen, X., Wang, K., Liu, M., Pei, R.: Hydrophobic IR-780 dye encapsulated in cRGD-conjugated solid lipid nanoparticles for NIR imaging-guided photothermal therapy. ACS Appl. Mater. Interfaces. **9**, 12217–12226 (2017)
19. Heck, J.G., Napp, J., Simonato, S., Möllmer, J., Lange, M., Reichardt, H.M., Staudt, R., Alves, F., Feldmann, C.: Multifunctional phosphate-based inorganic-organic hybrid nanoparticles. JACS **137**, 7329–7336 (2015)
20. Meng, F., Wang, J., Ping, Q., Yeo, Y.: Quantitative assessment of nanoparticle biodistribution by fluorescence imaging, revisited. ACS Nano **12**, 6458–6468 (2018)
21. Gravier, J.J., Garcia, F.P.N.Y., Delmas, T., Mittler, F., Couffin, A.-C., Vinet, F., Texier-Nogues, I.: Lipidots: competitive organic alternative to quantum dots for in vivo fluorescence imaging. J. Biomed. Opt. **16**, 096013 (2011)
22. Yukawa, H., Baba, Y.: In vivo fluorescence imaging and the diagnosis of stem cells using quantum dots for regenerative medicine. Anal. Chem. **89**, 2671–2681 (2017)
23. Li, J., Liu, F., Shao, Q., Min, Y., Costa, M., Yeow, E.K., Xing, B.: Enzyme-responsive cell-penetrating peptide conjugated mesoporous silica quantum dot nanocarriers for controlled release of nucleus-targeted drug molecules and real-time intracellular fluorescence imaging of tumor cells. Adv. Healthc. Mater. **3**, 1230–1239 (2014)
24. Anselmo, A.C., Mitragotri, S.: Nanoparticles in the clinic. Bioeng. Transl. Med. **1**, 10–29 (2016)
25. Kailasa, S.K., Koduru, J.R.: Perspectives of magnetic nature carbon dots in analytical chemistry: from separation to detection and bioimaging. Trends Environ. Anal. Chem. **33**, 00153 (2022)
26. Phua, V.J.X., Yang, C.T., Xia, B., Yan, S.X., Liu, J., Aw, S.E., He, T., Ng, D.C.E.: Nanomaterial Probes for Nuclear Imaging. Nanomaterials **12**(4), 582 (2022)
27. Baker, S.N., Baker, G.A.: Luminescent carbon nanodots: emergent nanolights. Angew. Chem. Int. Ed. **49**, 6726–6744 (2010)
28. Lim, S.Y., Shen, W., Gao, Z.: Carbon quantum dots and their applications. Chem. Soc. Rev. **44**, 362–381 (2015)
29. Li, H., Kang, Z., Liu, Y., Lee, S.-T.: Carbon nanodots: synthesis, properties and applications. J. Mater. Chem. **22**, 24230–24253 (2012)
30. Kateshiya, M.R., Malek, N.I., Kailasa, S.K.: Green fluorescent carbon dots functionalized MoO3 nanoparticles for sensing of hypochlorite. J. Mol. Liq. **351**, 118628 (2022)
31. Lesani, P., Lu, Z., Singh, G., Mursi, M., Mirkhalaf, M., New, E.J., Zreiqat, H.: Influence of carbon dot synthetic parameters on photophysical and biological properties. Nanoscale **13**, 11138–11149 (2021)
32. Đorđević, L., Arcudi, F., Cacioppo, M., Prato, M.: A multifunctional chemical toolbox to engineer carbon dots for biomedical and energy applications. Nat. Nanotechnol. **17**(2), 112–130 (2022)
33. Singh, A., Wolff, A., Yambem, S.D., Esmaeili, M., Riches, J.D., Shahbazi, M., Feron, K., Eftekhari, E., Ostrikov, K., Li, Q.: Biowaste-derived, self-organized arrays of high-performance 2D carbon emitters for organic light-emitting diodes. Adv. Mater. **32**, 1906176 (2020)
34. Singh, A., Eftekhari, E., Scott, J., Kaur, J., Yambem, S., Leusch, F., Wellings, R., Gould, T., Ostrikov, K., Sonar, P.: Carbon dots derived from human hair for ppb level chloroform sensing in water. Sustain. Mater. Tech. **25**, e00159 (2020)
35. Molaei, M.J.: Carbon quantum dots and their biomedical and therapeutic applications: a review. RSC Adv. **9**(12), 6460–6481 (2019)
36. Xu, Q., Kuang, T., Liu, Y., Cai, L., Peng, X., Sreeprasad, T.S., Zhao, P., Yu, Z., Li, N.: Heteroatom-doped carbon dots: synthesis, characterization, properties, photoluminescence mechanism and biological applications. J. Mater. Chem. B **4**, 7204–7219 (2016)
37. Yang, S., Sun, J., Li, X., Zhou, W., Wang, Z., He, P., Ding, G., Xie, X., Kang, Z., Jiang, M.: Large-scale fabrication of heavy doped carbon quantum dots with tunable-photoluminescence and sensitive fluorescence detection. J. Mater. Chem. A **2**, 8660–8667 (2014)
38. Nallayagari, A., Sgreccia, E., Pizzoferrato, R., Cabibbo, M., Kaciulis, S., Bolli, E., Pasquini, L., Knauth, P., Di Vona, M.: Tuneable properties of carbon quantum dots by different synthetic methods. J. Nanostruct. Chem. (2021). https://doi.org/10.3390/molecules27061832
39. Wang, B., Lu, S.: The light of carbon dots: from mechanism to applications. Matter **5**(1), 110–149 (2022)
40. Lan, M., Zhao, S., Zhang, Z., Yan, L., Guo, L., Niu, G., Zhang, J., Zhao, J., Zhang, H., Wang, P.: Two-photon-excited near-infrared emissive carbon dots as multifunctional agents for fluorescence imaging and photothermal therapy. Nano Res. **10**, 3113–3123 (2017)
41. Li, Y., Bai, G., Zeng, S., Hao, J.: Theranostic carbon dots with innovative NIR-II emission for in vivo renal-excreted optical imaging and photothermal therapy. ACS Appl. Mater. Interfaces **11**, 4737–4744 (2019)
42. Liu, R., Zhang, L., Zhao, J., Hou, C., Huang, Y., Huang, Z., Zhao, S.: A distinctive spinach-based carbon nanomaterial with chlorophyll-rich and near-infrared emission for simultaneous in vivo biothiol imaging and dual-enhanced photodynamic therapy of tumor. Adv. Ther. **2**, 1900011 (2019)
43. Liyanage, P.Y., Zhou, Y., Al-Youbi, A.O., Bashammakh, A.S., El-Shahawi, M.S., Vanni, S., Graham, R.M., Leblanc, R.M.: Pediatric glioblastoma target-specific efficient delivery of gemcitabine across the blood–brain barrier via carbon nitride dots. Nanoscale **12**, 7927–7938 (2020)
44. Shuang, E., Mao, Q.-X., Wang, J.-H., Chen, X.-W.: Carbon dots with tunable dual emissions: from the mechanism to the specific imaging of endoplasmic reticulum polarity. Nanoscale **12**, 6852–6860 (2020)
45. Liu, H., Sun, Y., Li, Z., Yang, J., Aryee, A.A., Qu, L., Du, D., Lin, Y.: Lysosome-targeted carbon dots for ratiometric imaging of formaldehyde in living cells. Nanoscale **11**, 8458–8463 (2019)
46. Ankireddy, S.R., Vo, V.G., An, S.S.A., Kim, J.: Solvent-free synthesis of fluorescent carbon dots: an ecofriendly approach for the bioimaging and screening of anticancer activity via caspase-induced apoptosis. ACS Appl. Bio Mater. **3**, 4873–4882 (2020)
47. Bao, Y.-W., Hua, X.-W., Li, Y.-H., Jia, H.-R., Wu, F.-G.: Hyperthemia-promoted cytosolic and nuclear delivery of copper/carbon

quantum dot-crosslinked nanosheets: multimodal imaging-guided photothermal cancer therapy. ACS Appl. Mater. Interfaces **10**, 1544–1555 (2018)
48. Tong, L., Wang, X., Chen, Z., Liang, Y., Yang, Y., Gao, W., Liu, Z., Tang, B.: One-step fabrication of functional carbon dots with 90% fluorescence quantum yield for long-term lysosome imaging. Anal. Chem. **92**, 6430–6436 (2020)
49. Qu, S., Wang, X., Lu, Q., Liu, X., Wang, L.: A biocompatible fluorescent ink based on water-soluble luminescent carbon nanodots. Angew. Chem. Int. Ed. **51**, 12215–12218 (2012)
50. Xu, J., Wang, C., Li, H., Zhao, W.: Synthesis of green-emitting carbon quantum dots with double carbon sources and their application as a fluorescent probe for selective detection of Cu^{2+} ions. RSC Adv. **10**, 2536–2544 (2020)
51. Yang, P., Zhu, Z., Chen, W., Luo, M., Zhang, W., Zhang, T., Chen, M., Zhou, X.: Nitrogen/sulfur Co-doping strategy to synthesis green-yellow emitting carbon dots derived from xylose: toward application in pH sensing. J. Lumin. **227**, 117489 (2020)
52. Lakowicz, J.R.: Principles of fluorescence spectroscopy. Springer, New York (2006)
53. Loi, E., Ng, R.W.C., Chang, M.M.F., Fong, J.F.Y., Ng, Y.H., Ng, S.M.: One-pot synthesis of carbon dots using two different acids and their respective unique photoluminescence property. J. Lumin. **32**, 114–118 (2017)
54. Zhou, F., Feng, H., Fang, Y., Sun, Q., Qian, Z.: Phenylsulfonic acid functionalized carbon quantum dots based biosensor for acetylcholinesterase activity monitoring and inhibitor screening. RSC Adv. **6**, 105454–105460 (2016)
55. Ferrari, A.C., Basko, D.M.: Raman spectroscopy as a versatile tool for studying the properties of graphene. Nat. Nanotechnol. **8**, 235–246 (2013)
56. Banun, V.J., Rewatkar, P., Chaudhary, Z., Qu, Z., Janjua, T., Patil, A., Wu, Y., Ta, H.T., Bansal, N., Miles, J.A.: Protein nanoparticles for enhanced oral delivery of coenzyme-Q10: in vitro and in silico studies. ACS Biomater. Sci. Eng. (2021). https://doi.org/10.1021/acsbiomaterials.0c01354
57. Chen, R., Liu, G., Sun, X., Cao, X., He, W., Lin, X., Liu, Q., Zhao, J., Pang, Y., Li, B.: Chitosan derived nitrogen-doped carbon dots suppress osteoclastic osteolysis via downregulating ROS. Nanoscale **12**, 16229–16244 (2020)
58. Esmaeili, M., Wu, Z., Chen, D., Singh, A., Sonar, P., Thiel, D., Li, Q.: Composition and concentration-dependent photoluminescence of nitrogen-doped carbon dots. Adv. Powder Technol. **33**, 103560 (2022)
59. Meng, X., Chang, Q., Xue, C., Yang, J., Hu, S.: Full-colour carbon dots: from energy-efficient synthesis to concentration-dependent photoluminescence properties. ChemComm. **53**, 3074–3077 (2017)
60. Smith, A.M., Mancini, M.C., Nie, S.: Second window for in vivo imaging. Nat. Nanotechnol. **4**, 710–711 (2009)
61. Wang, S., Li, B., Zhang, F.: Molecular fluorophores for deep-tissue bioimaging. ACS Cent. Sci. **6**, 1302–1316 (2020)

Authors and Affiliations

Amandeep Singh[1,2] · Zhi Qu[2] · Astha Sharma[3] · Mandeep Singh[4] · Brian Tse[5] · Kostya Ostrikov[1,2] · Amirali Popat[6] · Prashant Sonar[1,2] · Tushar Kumeria[3,6,7]

✉ Prashant Sonar
sonar.prashant@qut.edu.au

✉ Tushar Kumeria
t.kumeria@unsw.edu.au

[1] School of Chemistry and Physics, Queensland University of Technology, Brisbane, QLD 4000, Australia

[2] Centre for Materials Science, Queensland University of Technology, Brisbane, QLD 4000, Australia

[3] School of Materials Science and Engineering, University of New South Wales, Sydney, NSW 2052, Australia

[4] School of Science, RMIT University, Melbourne, VIC 3000, Australia

[5] Preclinical Imaging Facility, Translational Research Institute, Brisbane 4102, Australia

[6] School of Pharmacy, University of Queensland, Brisbane, QLD 4102, Australia

[7] Australian Centre for Nanomedicine, University of New South Wales, Sydney, NSW 2052, Australia